Supplementary Material to "Thermodynamically complete equation of state of MgO from true radiative shock temperature measurements on samples preheated to 1850 K"

O. V. Fat'yanov,* P. D. Asimow,† and T. J. Ahrens‡

Division of Geological and Planetary Sciences 252-21,

California Institute of Technology, Pasadena, CA 91125, U.S.A.

(Dated: December 13, 2017)

I. EXPERIMENTAL APPROACH

A. Salient features of particular experiments

Shots #383 and #384 were done using an irradiance-type shock pyrometer calibration,[1,2] with post-shot determination of the actual calibration factors for each of 4 pyrometer channels operating at 502, 602, 755, and 909 nm wavelengths. The diameter of the high-precision aperture in the Mo cap for these experiments was 2.959 ± 0.013 mm, as measured at ambient conditions with specially machined go – no go plugs. No Ti foil between the Mo driver plate and the MgO crystal was used in these experiments.

Shot #387 was the first done with the new radiance-type shock pyrometer calibration.[2,3] The target aperture diameter was increased to 4.5 mm (at ambient conditions), whereas the area probed by the shock pyrometer was 2.5 mm in diameter. All 6 channels were used, operating at 502, 602, 662, 755, 832, and 909 nm wavelengths. As in shots #383 and #384, no Ti foil was used to seal the gap between the MgO crystal and Mo capsule bottom. Due to operational difficulties, the target was held at 1300 K for 2 hours before the experiment, whereas normally the total heating cycle is only several minutes.

Shot #389 was a repeat of #387 without the lengthy preheat period. It yielded very similar temperature data.

Shots #389 and #390 were the first to employ a 13 μm thick Ti foil that completely masked any non-equilibrium light flash caused by the shock wave closing the gap between the Mo driver plate and MgO sample. However, in these experiments we observed a 60 K decrease in radiative temperature over the last 70 ns of shock travel in the MgO, attributed to insufficient thermal contact between the sample back surface and hot Mo cap.

Shot #391 was the only experiment done with 2 layers of thin Ti foil. One disk was placed between the Mo capsule bottom and the MgO crystal impact face, as in shots #387-390. An additional annulus with an aperture in the center roughly equal to the aperture in Mo cap was installed between the rear face of the MgO crystal and the cap. We expected some improvement of thermal contact between the MgO rear face and hot Mo cap. However, intense evaporation of Ti and chemical reaction with hot MgO resulted in partial darkening of the initially transparent MgO crystal in the area viewed by the shock pyrometer. This was evident due to the unique, nearly linearly increasing radiative temperature profile in

this particular experiment, with the T value expected for this shot's pressure observed only upon shock wave arrival at the MgO free surface.

Shots #405 and #406 were done at nearly the same impact velocity to measure shock front reflectivity. Shot #405 employed the same target configuration as shots #389 and #390 (Figure 2a of the main paper). Shot #406 used an MgO crystal half as thick (1.5 mm vs. 3 mm) backed by a stack of 5 thin sapphire windows with Mo foil spacers (Figure 2b of the main paper).

Shot #407 was done with a reduced distance (2 mm vs. 3.5 mm in all previous experiments) between the Mo driver plate and the Cu heating coil. The other difference from all previous experiments was the use of a single oscilloscope channel for each pyrometer channel (no back-up scope channels). We expected that the new coil placement would reduce the gradual increase in electronic output signals as the shock propagated through the sample. However, this experiment instead yielded the steepest such upwards brightness ramp. Moreover, this was the first experiment that yielded poor agreement between values of radiative temperature determined from the absolute light intensity (so-called brightness T) and from the shape of the emission spectrum (so-called color T). The brightness temperature was 8800 K, which corresponds to 9500 K true temperature after reflectivity correction, while the color temperature was only 8300 K for unweighted and 8700 K for weighted fits.

Shot #408 was assembled and executed at nearly the same conditions and was designed to repeat shot #407. However, instead of observing a shock temperature closer to the value predicted for the shot pressure, we recorded a dramatically lower light intensity on all 6 pyrometer channels. We believe this intensity loss was caused by misalignment of the front surface turning mirror. The brightness (5700 K to 6100 K) and color temperatures (7100 K unweighted and 10500 K weighted fits) from this shot did not agree with each other. However, the sign of the difference was opposite to that observed in shot #407.

Shots #410 and #411, the last experiments of this series, were done to measure shock front reflectivity at the highest attainable pressure. These experiments were very similar to #405 and #406 except for higher impact velocity (7.5 km/s vs. 6.9 km/s) and the shortest distance (1.5 mm vs. 3.5 mm) between the heating coil and Mo capsule driver plate.

B. Thermal gradients in hot MgO targets

Thermal gradients in the samples were measured with a Williamson two-color pyrometer with 2.5 mm diameter spot size. Several tests were performed using both target configurations (see Figure 2 of the main paper). The temperature distribution across the driver surface was mapped using empty Mo capsules; that on the rear surface of the MgO was mapped using 25 μm thick Mo foil to form a radiating surface. The extra piece of foil causes negligible perturbations to the induction coupling and temperature fields. It absorbs less than 10^{-3} of total EM power delivered to the target assembly by the RF heater (i.e., less than c.a. 1.5 W of additional power) and we estimate at most a few K difference in the temperature distribution anywhere in the target.

The results indicated an upper limit of +3 to +7 K/mm for the longitudinal temperature gradient (downrange free surface hotter than driver surface) in the configuration used in shots #383-#406, where the central plane of the heating coil was placed 3.5 mm downrange of the Mo driver plate surface. In experiments with shorter driver-to-coil distances (1.5 mm for shots #410-411 and 2 mm for shots #407-408), we observed -25 to -30 K/mm negative gradients (i.e. driver plate side hotter than downrange free surface). We measured lateral gradients of ~20 K/mm over the downrange free surface of MgO crystals, with T increasing outwards from the center towards the Mo aperture edge and roughly uniform azimuthal distribution. The lateral temperature distribution was nearly the same for both unwindowed and windowed target configurations and any position of the coil. Lateral gradients near the impact face of MgO crystals in contact with hot Mo driver plate did not exceed 10 K/mm and also exhibited azimuthal uniformity. These gradients have negligible impact on the accuracy of radiative temperature and shock speed measurements in all our experiments that viewed the central 2.5 mm diameter area of 1.5 or 3 mm long MgO samples. Simultaneous measurements of hot target temperatures with two Williamson pyrometers, our older instrument with 19 mm diameter spot and our newer instrument with 2.5 mm spot, revealed that initial MgO temperatures are ~65-70 K lower than those we reported in Ref. 3.

C. Degradation of front-surface turning mirrors

Values of the thermal damage threshold specified by the vendor for the front surface turning mirrors (protected silver, PF10-03-P01 from Thorlabs, Inc.) used to deliver light from targets to the shock pyrometer, 1750 W/cm at 1.064 μm wavelength and 1500 W/cm at 10.6 μm, are about 10 times higher than the maximum linear power density of the entire radiation spectrum received by the mirror from our targets preheated to 1850 K. However, special tests of the mirror performance before and after it was exposed for a few seconds to heat from the hot target revealed up to 15% reduction of the mirror reflectivity, wavelength independent within the uncertainty and reproducibility of these measurements. An average 6.4% reduction of reflectivity for all pyrometer channels (or absolute intensity correction factor of 0.936) was determined for the type of turning mirrors employed in the whole 1850 K series of our experiments.

II. HUGONIOTS AND GRÜNEISEN MODEL

A. Room-T Hugoniot analysis

Independence of our fitting parameters for MgO room-T U vs. D Hugoniot (the counterpart of Table I from the main paper) is shown in Table I.

B. Other Grüneisen model candidates

A comparison of ten different $\gamma(V)$ models for metallic (Cu, Fe, K) and ionic (NaCl, MgO) solids was reported recently.[4] The author discussed applicability of that models for the description of shock-wave EOS results but checked them mainly against the room-T data obtained from static compression measurements only (Cu, Fe, K) or primarily from computer simulations (MgO). Only for NaCl the models were checked against the high temperature (up to 500° C) static compression data.[4] Therefore, it was essential to redo this type of analysis for MgO using the proper Grüneisen values from our preheated shock experiments.

Our results are summarized in Table II. The absolute reduced misfit χ^2 was computed exactly the same way as in the main paper (via Equation 3 of Ref. 5). That means the values listed in the last column of Table II can be directly compared to the χ^2 data from Table IV

TABLE I. Comparison of the *inverted* maximum likelihood principal Hugoniots for MgO obtained from the U vs. D and D vs. U fits. Insignificant digits are shown to emphasize the differences. The opposite sign of absolute slope and intercept differences confirms strong anti-correlation of the best linear fit parameters. The reduced misfit was calculated for $n = 20$ data points and $q = 2$ parameters or $(n - q) = 18$ degrees of freedom.

Parameter	U vs. D fit	D vs. U fit	Absolute difference
Intercept, A	-4.89960	-4.90959	-0.0100
Intercept uncertainty, σ_A	0.083762	0.083896	1.33×10^{-4}
Slope, B	0.738282	0.739175	0.000893
Slope uncertainty, σ_B	0.0075163	0.0075284	1.21×10^{-5}
Uncertainty correlation, $cor(\sigma_A, \sigma_B)$	-0.994378	-0.994386	-8.1×10^{-6}
Absolute reduced misfit, $\chi_0^2/(n-q)$	0.182551	0.182478	-7.3×10^{-5}

of the main paper. Our analysis was done for $n = 12$ data points and $q = \{3, 4, 5, 6\}$ total number of model parameters (one to four parameters for the $\gamma(V)$ functions considered here plus two more for linear shock velocity vs. particle velocity 1850 K Hugoniot) or $(n - q) = \{9, 8, 7, 6\}$ degrees of freedom for the final fit.

It is clear that none of these additional Grüneisen models fits our data significantly better than the three models we already tested (the last column of Table II). Only two of 11 additional functions show the reduced misfits just slightly lower than that for $\gamma = \gamma_0 \times V/V_0$ model. None of these extra models performs better than the functions of Al'tshuler and Molodets examined in the main paper. In fact, there is no improvement of fit if one adds more adjustable parameters. This is especially clear after comparison of the best-fit values for the Anderson's power law (2 parameters), general Al'tshuler's formula (3 parameters), and the most sophisticated Stacey and Davis (4 parameters) functions. It appeared that the absolute minima conditions for these models are achieved if the redundant parameters (γ_∞ for the Al'tshuler's and λ_0 for Stacey and Davis' functions, respectively) are nullified. This reduces all three best-fit functions to the same form of Anderson's simple two-parameter formula with the power of $q_0 = 0.988$ (Table II) which is just 1.2% different from our preferred model value of $q_0 = 1$. While the absolute misfits are equal in all three cases, the reduced misfits are different because the number of fitting parameters q increases from 4 for

TABLE II. Comparison of 1850 K MgO linear Hugoniot fits for other reported Grüneisen models.

Author(s)	$\gamma(V)$ model	Best-fit parameters	Reduced χ^2
Bennett et al.[6]	$\gamma = \gamma_0 V/V_0 + \frac{2}{3}(1 - V/V_0)$	$\gamma_0 = 1.154$	0.97
Thomson and Lawson[7]	$\gamma = \gamma_0 V/V_0 + \frac{2}{3}(1 - V/V_0)^2$	$\gamma_0 = 1.313$	0.99
Rice[8]	$\gamma = \gamma_0 V/V_0 \times [1+\gamma_0(1 - V/V_0)]^{-1}$	$\gamma_0 = 2.202$	1.78
Royce[9]	$\gamma = \gamma_0 - a(1 - V/V_0)$	$\gamma_0 = 1.347$ $a = 1.288$	1.12
Anderson[10]	$\gamma = \gamma_0 \times (V/V_0)^{q_0}$	$\gamma_0 = \mathbf{1.366}$ $q_0 = \mathbf{0.988}$	**1.14**
Srivastava and Sinha[11]	$\gamma = \gamma_0 \times exp\left\{ln(2\gamma_0) \times [(V/V_0)^{q_0} - 1]\right\}$	$\gamma_0 = 1.747$ $q_0 = 1.864$	1.23
Gospodinov[4]	$\gamma = \gamma_0 \times exp\left\{ln(\frac{3}{2}\gamma_0) \times [(V/V_0)^{q_0} - 1]\right\}$	$\gamma_0 = 2.723$ $q_0 = 3.949$	1.32
Jeanloz[12]	$\gamma = \gamma_0 \times exp\left\{\frac{q_0}{q'} \times [(V/V_0)^{q'} - 1]\right\}$	$\gamma_0 = 1.060$ $q_0 = 0.099$ $q' = -4.410$	1.19
Al'tshuler and Sharipdzhanov[13]	$\gamma = \gamma_\infty + (\gamma_0 - \gamma_\infty) \times (V/V_0)^{q_0}$	$\gamma_0 = \mathbf{1.366}$ $\gamma_\infty = 0$ $q_0 = \mathbf{0.988}$	**1.31**
Khishenko et al.[14]	$\gamma = 2/3 + (\gamma_0 - 2/3) \times \frac{\sigma_n^2 + ln^2(\sigma_m)}{\sigma_n^2 + ln^2(V_0/(V \times \sigma_m))}$	$\gamma_0 = 1.304$ $\sigma_n = 0.187$ $\sigma_m = 0.472$	1.18
Stacey and Davis[15]	$\gamma = \gamma_0 \times \left[\frac{\lambda_0}{\lambda_\infty} - \left(\frac{\lambda_0}{\lambda_\infty} - 1\right) \times \left(\frac{V}{V_0}\right)^{\lambda_\infty}\right]^{-q_0/(\lambda_0 - \lambda_\infty)}$	$\gamma_0 = \mathbf{1.366}$ $\lambda_0 = 0$ $\lambda_\infty \neq 0$ $q_0 = -\mathbf{0.988}$	**1.52**

the Anderson's model to 6 for the Stacey and Davis's model.

III. VALIDATION OF OUR GRÜNEISEN MODEL

Figure 1 shows the plots of the most popular semi-empirical $\gamma(V)$ functions reported for the EOS constructed from static compression data only or from both static and shock data. The results of pure theoretical or computational predictions were intentionally excluded from this analysis because of too high systematic errors exhibited by the majority of such data.

The plots in Figure 1 can be approximately divided into 3 major groups that are (1) well consistent (Refs. 16–18 and Ref. 19, unconstrained fit), (2) not so consistent (Ref. 19, fixed K'_T fit; Ref. 22, 3BM EOS model; Ref. 23, Al'tshuler $\gamma(V)$ model; and Refs. 20, 21, and 24),

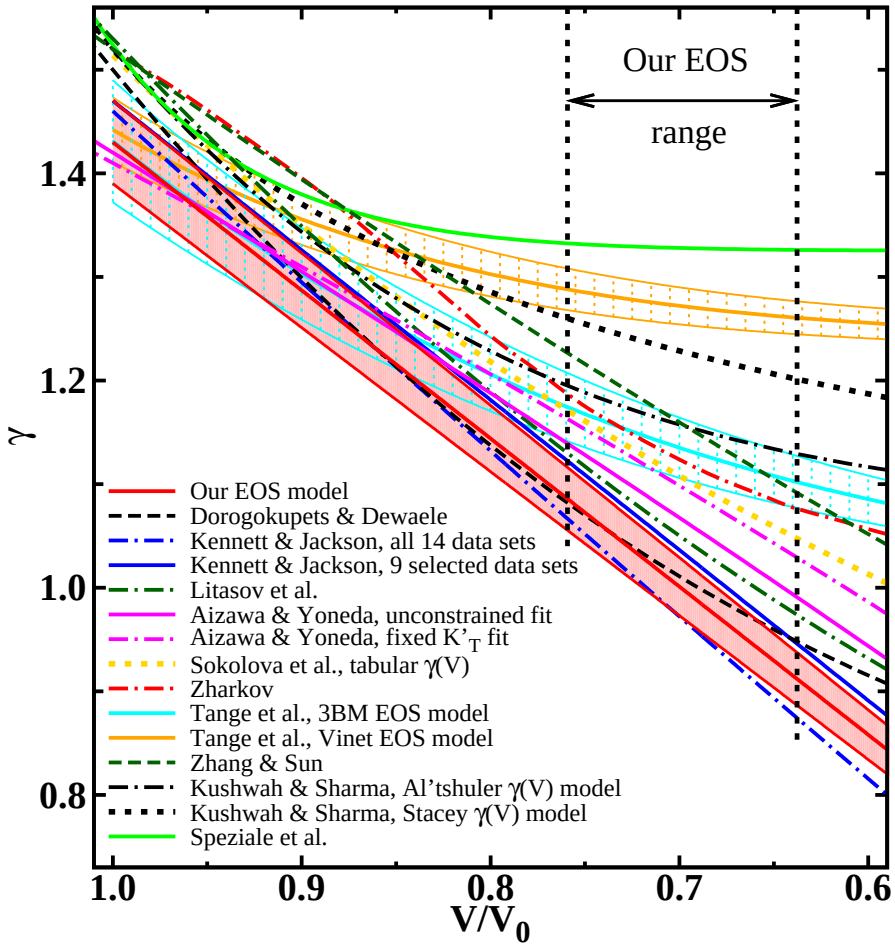

FIG. 1. Comparison of our $\gamma(V)$ model with the reported semi-empirical models for MgO from static compression data only or from both static and shock compression data.[16–25] The shaded areas are the reported 1σ uncertainties.

and (3) definitely inconsistent (Ref. 22, Vinet EOS model; Ref. 23, Stacey $\gamma(V)$ model; and Ref. 25) with our data. As was already discussed in the main paper, the best agreement with our Grüneisen function was demonstrated by the model of Dorogokupets and Dewaele[16] and by both maximum-likelihood models of Kennett and Jackson.[17] The reported uncertainties for the latter models[17] (not shown in Figure 1 to avoid obscuration of other curves) are roughly equal to those for our data. It appeared that none of the MgO Grüneisen models shown in Figure 1 is capable of predicting both $\gamma(V)$ *at high pressure* and $\gamma(T)$ *at 1 bar* with the accuracy of our function or at least of those constructed by Kennett and Jackson.[17]

IV. EXAMPLE OF NON-REFLECTING SHOCK

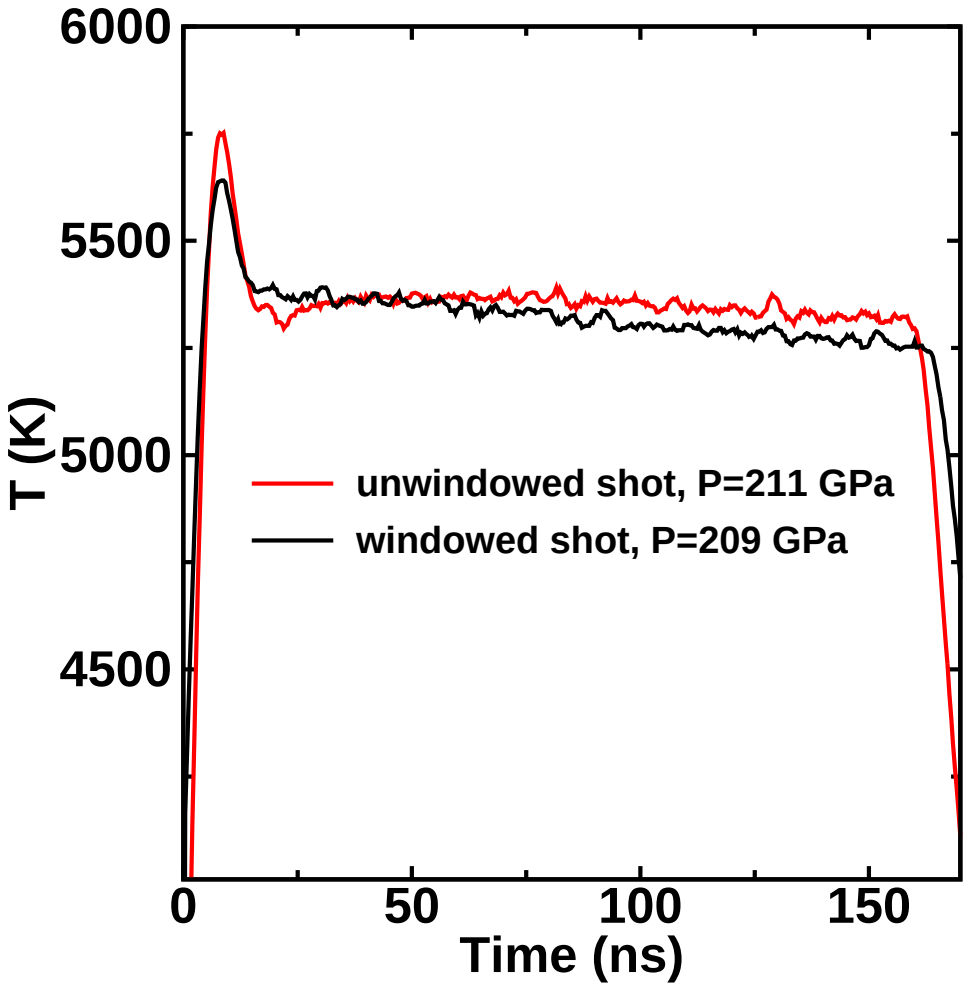

FIG. 2. Brightness temperature profiles ($r = 0.016$) from two shots done with the same pyrometer settings and at nearly the same impact velocity. Noise on records indicates the level of data precision. Both profiles match over the overlapped portions of both records from 30 to 60 ns. A slow decrease of shock T from both records after c.a. 70-100 ns suggests incomplete melting of forsterite in that experiments.

V. CUMULATIVE DESCRIPTION OF SEPARATE ASCII DATA FILES

A. room-T Hugoniot

The following ASCII files in the "./298_K/" subdirectory are the primary data used for the D vs. U fitting: "*MgO-Carter-1980*",[26] "*MgO-Fratanduono-2013*",[27] "*MgO-Vassiliou-1981*",[28] and "*MgO-Zhang-2008*".[29] All these files have 4 columns of U, D, σ_U, and σ_D values except for the first 2-column file of "*MgO-Carter-1980*" that lists U and D only. All the velocities and their uncertainties are in km/s. Two high-pressure experiments of Fratanduono et al.[27] yielded 2 pairs of statistically independent, yet equal Hugoniot points that were included altogether in our analysis. The data that show two-wave structure, with $U < 2$ km/s or $D < 9.8$ km/s, were rejected by the fitting program. The remaining 21 points with assigned uncertainties used for the room-T Hugoniot analysis are listed in the "*MgO-298K-sum*" and the corresponding maximum likelihood U and D data are listed in the "*MgO-298K-fit*". Both files have the same 4-column format specified above.

B. Thermodynamic parameters of MgO required for the EOS construction

1. Heat capacity at 1 bar ("./thermo/Cp/" subdirectory)

The as reported tabular data for molar heat capacity are listed in files "*WANG-Cp-table*",[31] and "*NIST-Cp-table*".[30] The results of our cubic-spline interpolation of these data are listed, respectively, in files "*WANG-Cp*", and "*NIST-Cp*". Two more files, "*SAXENA-Cp-formula*" and "*JACOBS-Cp-formula*", list the values computed from the reported best-fit expressions[32,33].

All the files in this subdirectory have 2 columns: (1) T $[K]$ and (2) C_p $[J/(mol \times K)]$. The only minor exception is the "*WANG-Cp-table*" file with the original C_p data given in $[cal/(mol \times K)]$). Conversion of a molar heat capacity $[J/(mol \times K)]$ to a regular specific heat $[J/(kg \times K)]$ requires division of all tabulated here values of C_p by the molar weight of MgO in kilograms, $M = 0.0403$.

2. *Thermal expansion at 1 bar ("./thermo/alpha/" subdirectory)*

All the thermal expansion data used in our analysis are listed in five ASCII files with 2 columns: (1) T $[K]$ and (2) dimensionless volume $\alpha \times 1e6$. These include the as reported tabular values of Wang & Reeber[31] (file "*WANG-alpha-table*") and the relevant $\alpha(T)$ data computed (1) by cubic-spline interpolation (file "*WANG-alpha*") or (2) using the reported formulas[34–36] (files "*JACOBS-alpha-formula*", "*DUBROVINSKY-alpha-formula*", and "*FIGUET-alpha-formula*").

3. *Adiabatic bulk modulus Ks(T) ("./thermo/Ks/" subdirectory)*

Two files, "*SUMINO-Ks-table*" and "*ISAAK-Ks-table*", list the published tabular data[40,41] in 3-column format: (1) T $[K]$, (2) $Ks(T)$ $[GPa]$, and (3) σ_{Ks} $[GPa]$. The file "*ZOUBOLIS-Ks-formula*" lists $Ks(T)$ data computed from the reported best-fit expressions for MgO elastic constants.[42] It has 2-column format: (1) T $[K]$ and (2) $Ks(T)$ $[GPa]$. All these data were used to compute $\gamma(T)$ at 1 bar required for our Grüneisen model validation against available experimental values (Section III D 3 of the main paper).

4. *The main data used to construct our EOS ("./thermo/" subdirectory)*

The following three 5-column files have the most essential MgO parameters and their estimated uncertainties tabulated from 298 to 2400 K in 1 K increment. "*MgO-alpha-X*" lists T $[K]$, and 4 dimensionless quantities: volume thermal expansion $\alpha = \partial ln(V)/\partial T$, its uncertainty σ_α, ratio $x = V(T)/V_0$ (V_0 is MgO volume at 298 K), and its uncertainty σ_x. "*MgO-Rho-V*" lists T $[K]$, ρ $[g/cm^3]$, σ_ρ $[g/cm^3]$, $V = 1/\rho$ $[cm^3/g]$, and σ_V $[cm^3/g]$. Both files were generated from 4 data sets found in the " *./thermo/alpha/* " subdirectory. "*MgO-Cp-dE*" lists T $[K]$, C_p $[J/g/K]$, σ_{C_p} $[J/g/K]$, $\Delta E = E(T) - E_0$ $[J/g]$ ($E_0 = E(298\ K)$), and $\sigma_{\Delta E}$ $[J/g]$. This file was generated from 4 data sets located in the " *./thermo/Cp/* " subdirectory.

C. Representative results of 1850 K data analysis ("./1850_*K*/" subdirectory)

The values plotted in the upper panel of Figure 3 from the main paper are listed in "*gamma_*01.*dat*" file. It has 5 columns of data: (1) U_1 $[km/s]$, (2) U_2 $[km/s]$, (3) volume of 1 g of compressed MgO V $[cm^3]$, (4) apparent γ_0, and (5) $\gamma = \gamma_0 \times V/V_0$. We also included a similar file "*gamma_*00.*dat*" that lists the same parameters for the analysis done without applying any Grüneisen model, as described in Section III B of the main paper and shown in the first line of Table IV there. Files "*CONST-T* ", "*ALTSHULER-T* ", "*MOLODETS-T* ", and "*GAMMA-T* " have data on temperature dependence at 1 bar for the 4 best-fit Grüneisen functions with the parameters listed in rows #2 to #5 of Table IV from the main paper. Each file has 2-columns: (1) T $[K]$ and (2) dimensionless $\gamma(T)$.

D. Prediction of hot Hugoniots

1. *Uncertainties and their correlations ("./synthetic/sigma/*1e5*_points/" and "./synthetic/sigma/*1e6*_points/" subdirectories)*

Each of these directories has 27 files with the names automatically generated from the values of U_1 with omitted dots. The files in subdirectory "./*synthetic/sigma/*1e5*_points/*", for example, have the following names: "*U1_22_1e5*", "*U1_23_1e5*", "*U1_24_1e5*", ... "*U1_47_1e5*", and "*U1_48_1e5*". Most information there is self-explanatory including the name postfix that indicates the total number of points used to build the histograms. The first 4 lines in each file are the parameters for the Grüneisen coefficients γ_0 (denoted in ASCII as $g0$) and γ (denoted in ASCII as g) and linear hot Hugoniot intercepts c_2 and slopes s_2. We used c_2 and s_2 here instead of a_2 and b_2 to distinguish between the experimental and synthetic Hugoniot coefficients. Each line gives the amplitude of the histogram, the maximum likelihood synthetic value, and its uncertainty. Then there are 4 groups of correlation coefficients. The first group shows all 6 correlations between the uncertainties of parameters for the room-T (c_1, s_1) and 1850 K (c_2, s_2) Hugoniots. The second group lists 7 correlations between the uncertainties of γ and c_1, s_1, c_2, s_2, $r_1 = 1/V_{01}$, $r_2 = 1/V_{02}$, or ΔE (denoted as E in ASCII files). The third group is very similar to the second, it lists the same type of correlation coefficients for γ_0. The fourth group lists 6 correlations between γ_0, γ, V_{01} (denoted in ASCII as $v1$), and V.

2. *Synthetic (U, D) data ("./synthetic/" subdirectories)*

The primary arrays of numeric values can be found in 10 data files "*500.dat*", "*750.dat*", "*1000.dat*", ... "*2300.dat*", and "*2400.dat*" with the names matching the initial temperatures. Each file has 5 data columns: particle velocity U, its uncertainty σ_U, shock velocity D, its uncertainty σ_D, and correlation $cor(\sigma_U, \sigma_D)$. All the velocities and their uncertainties are in km/s.

The main results of constructing linear D vs. U functions from that primary values are summarized in files "*hug-all-1*", and "*hug-all-2*" with 6 columns of data: T, slope b, intercept a, σ_b, σ_a, and correlation $cor(\sigma_a, \sigma_b)$. Temperature T is in K, intercept a and its uncertainty σ_a are in km/s. The slope b and its uncertainty σ_b are dimensionless. The maximum likelihood intercepts a and slopes b included in Tables V and VI of the main paper were taken from both files, "*hug-all-1*" and "*hug-all-2*". The uncertainties of that parameters, σ_a and σ_b, were taken from "*hug-all-1*" only.

The file "*U2-min-max*" lists the model lower (U_2^{min}) and upper (U_2^{max}) limits of particle velocity versus the initial temperature. This information was reported on the last two lines of Table VI of the main paper. The file has 3 columns of data: (1) T $[K]$, (2) U_2^{min} $[km/s]$, and (3) U_2^{max} $[km/s]$.

E. Grüneisen functions ("./*gamma*/" subdirectory)

1. $\gamma(T)$ *models at 1 bar ("./gamma/T/" subdirectory)*

All the files in this subdirectory can be divided into 3 groups. The first group has as-reported tabular data (files "*SUMINO-T-table*",[40] "*ISAAK-T-table*",[41] and "*SOKOLOVA-T-table*",[20] or the values we extracted from the published data plots (files "*JACOBS-Debye-V-plot*", "*JACOBS-Debye-V-T-plot*", "*JACOBS-Kieffer-V-plot*", and "*JACOBS-Kieffer-V-T-plot*").[36]

The second group consists of $\gamma(T)$ sets that were constructed from a combination of directly measured thermodynamic parameters, without involving any particular Grüneisen models. Three files "*SUMINO-Ks*", "*ISAAK-Ks*", and "*ZOUBOLIS-Ks*" were generated from the reported $Ks(T)$ data[40–42] ("./*thermo*/*Ks*/" subdirectory) using our EOS values for $\alpha(T)$, $V(T)$, and $C_p(T)$ (files from the "./*thermo*/" subdirectory). File "*GAMMA-2*"

lists our $\gamma_2(T)$ values given by Equation 3 of the main paper and plotted in Figure 5 there.

All the files in the last group give $\gamma(T)$ values that were merely computed from the known $\gamma(V) = \gamma(V/V_0)$ models using our thermal expansion data (file "*./thermo/MgO-alpha-X*"). The files "*DOROGOKUPETS*",[16] "*KENNETT*",[17] "*LITASOV*",[18] "*SPEZIALE*",[25] and "*TANGE*"[22] were generated from the reported volume-dependent Grüneisen models. The file "*GAMMA-1*" lists the values of our primary $\gamma_1(T)$ function given by Equation 1 of the main paper and plotted in Figure 5 there.

The majority of files in this subdirectory have 2-column format: (1) T $[K]$, and (2) dimensionless $\gamma(T)$. Five files there, "*SUMINO-T-table*",[40] "*ISAAK-T-table*",[41] "*SUMINO-Ks*", "*ISAAK-Ks*", and "*ZOUBOLIS-Ks*" have 3-column format: (1) T $[K]$, (2) dimensionless $\gamma(T)$, and (3) dimensionless σ_γ. Each of two more 3-column files, "*KENNETT*" and "*TANGE*", includes two separate Grüneisen functions in the format of: (1) T $[K]$, (2) dimensionless $\gamma_1(T)$ (EOS model I), and (3) dimensionless $\gamma_2(T)$ (EOS model II).[17,22]

The maximum estimated absolute 1σ uncertainty for each of our primary $\gamma(T)$ models (Equations 1 and 3 of the main paper) was found approximately constant at ± 0.04 level. Therefore, no σ_γ data were included in the "*GAMMA-1*" and "*GAMMA-2*" files.

2. ***High pressure $\gamma(V)$ models: <u>shock</u> compression data ("./gamma/V/Shock" subdirectory)***

The files "*ALTSHULER-V*", "*CARTER-V*", and "*MOLODETS-V*" list the values generated from the reported $\gamma(V)$ functions.[13,37,38] "*GAMMA-V*" is our current EOS model. Dimensionless data for all these files are listed in 2-column format: (1) compression $x = V/V_0$ and (2) γ.

The original tabular $\gamma(V, E)$ data of Bushman and Lomonosov[39] relevant to our work are listed in 3-column files "*BUSHMAN-100-table*" and "*BUSHMAN-106-table*". Their format is: (1) specific volume V $[cm^3/g]$, (2) specific internal energy E [kJ/g], and dimensionless γ. The results of our cubic-spline interpolation of these data are listed, respectively, in files "*BUSHMAN-100*", and "*BUSHMAN-106*". They have 2-columns of dimensionless data: (1) sample compression $x = V/V_0$ and (2) γ.

The array of Grüneisen data in file "*BUSHMAN-V*" is an average of two γ values from "*BUSHMAN-100*" and "*BUSHMAN-106*" files. It has 3 columns of data: (1) compression

$x = V/V_0$, (2) γ, and (3) σ_γ. The uncertainty of Bushman and Lomonosov's Grüneisen function listed in the 3-rd column of file "*BUSHMAN-V*" was estimated as a root-mean square average of two values: (1) half the difference between the data from samples with $m = 1.00$ and $m = 1.06$ porosities (values of γ from the files "*BUSHMAN-100*" and "*BUSHMAN-106*") and (2) a constant relative systematic error of $\pm 3\%$ typical of our γ data.

3. *High pressure $\gamma(V)$ models: static compression data ("./gamma/V/Static" subdirectory)*

The files "*JACKSON1-V*" (inversion of all 14 data sets), "*JACKSON2-V*" (inversion of 9 data sets that do not depend on empirical pressure scales), "*TANGE-3BM-V*", and "*TANGE-Vinet-V*" list the values generated from the reported $\gamma(V)$ functions and uncertainties of their model parameters.[17,22] Dimensionless data are listed in 3-column format: (1) $x = V/V_0$, (2) γ, and (3) σ_γ.

The data of Zharkov digitized from the plot (file "*ZHARKOV-V-plot*") also has 3 columns: (1) dimensionless compression $x = V/V_0$ (recalculated by us from the density listed in column #3), (2) dimensionless γ, and (3) density ρ $[g/cm^3]$. The as reported tabular data of Sokolova et al.[20] are given in 2-column file "*SOKOLOVA-V-table*" of dimensionless data: (1) compression $x = V/V_0$ and (2) γ. Other data sets plotted in Figure 1 (see Section III above) were generated from the best-fit parameters reported in Refs. 15, 16, 18, 19, 23–25.

F. Shock temperatures ("./*shock_T*/" subdirectory)

1. *Calculated Hugoniot temperatures ("./shock_T/calc" subdirectory)*

Files "*298K*", "*1850K*", and "*2300K*" list on-Hugoniot shock T vs. P predicted by our EOS for the B1-phase MgO with the initial T_0 of 298 K, 1850 K, and 2300 K, respectively. As reported tabular shock T data of Root et al.[43] for B1 MgO samples with the initial temperature of $T_0 = 1900$ K are given in the file "*ROOT-1900K-table*". The results of our cubic-spline numerical interpolation ($0 \leq P \leq 228$ GPa) and extrapolation (to $P \leq 300$ GPa) of that data can be found in files "*ROOT-1900K*" and "*ROOT-1900K-extrapolation*", respectively. All the files in this subdirectory have 2 columns of data: (1) P

$[GPa]$ and (2) Hugoniot T $[K]$.

2. ***Our experimental data: <u>good</u> ("./shock_T/exper/good/brightness" and "./shock_T/exper/good/true" subdirectories)***

Ten files in each subdirectory list the main results of our experiments # 383, # 384, # 387, #389-391, #405, #406, #410, and #411. The names of files are self-explanatory: "*t383-br*", "*t384-br*", "*t387-br*", ... "*t410-br*", and "*t411-br*" in the "*/brightness*" subdirectory and "*t383-true*", "*t384-true*", "*t387-true*", ... "*t410-true*", and "*t411-true*" in the "*/true*" subdirectory. All brightness temperatures were extracted from the radiance data using the shock front reflectivity of $r = 0.02$. The true temperatures were computed for the shock front reflectivity of $r = 0.22$ in all the experiments except for #410 and #411 where $r = 0.21$ was used. All twenty files have 4-column data format: (1) time $[s]$, (2) T $[K]$, (3) estimated precision of T $[K]$, and (4) estimated full uncertainty of T $[K]$.

3. ***Our experimental data: <u>inconsistent</u> ("./shock_T/exper/inconsistent" subdirectory***

The results of formal analysis of data from two experiments #407 and #408 were included in this subdirectory for the completeness. Again, all four filenames ("*t407-r02*", "*t407-r22*", "*t408-r02*", and "*t408-r22*") are self-explanatory: each name includes the number of a particular experiment and the value of shock front reflectivity used for the analysis. Files "*t407-r02*" and "*t407-r22*" have the same 4-column format as the good data files discussed above. The data from experiment #408 (files "*t408-r02*" and "*t408-r22*") are shown in 2-column format only: (1) time $[s]$ and (2) T $[K]$.

---

* fatyan1@gps.caltech.edu

† asimow@gps.caltech.edu

‡ Passed away in 2010, before this work was completed

[1] S. C. Gupta, S. G. Love, and T. J. Ahrens, Earth Planet. Sci. Lett. **201**, 1 (2002).

[2] O. V. Fat'yanov and P. D. Asimow, Rev. Sci. Instr. **86**, 101502 (2015).

[3] O. V. Fat'yanov, P. D. Asimow, and T. J. Ahrens, in *Shock Compression of Condensed Matter – 2009: AIP Conference Proceedings 1195*, Nashville, Tennessee, U.S.A., 28 June – 3 July 2009, edited by M. L. Elert, W. T. Buttler, M. D. Furnish, W. W. Anderson, and W. G. Proud (American Institute of Physics, Melville, New York, 2009), pp. 855-858.

[4] V. Gospodinov, International Journal of Modern Physics B **28**, 1450196 (2014); "Volume dependence of the Grüneisen ratio for shock-wave equation-of-state studies," arXiv:1401.1041 (2014) available at *https://arxiv.org/pdf/1401.1041.pdf*

[5] O. V. Fat'yanov and P. D. Asimow, J. Appl. Phys. **121**, 115904 (2017).

[6] B. I. Bennett, J. D. Johnson, G. I. Kerley, and G. T. Root (1978) as discussed in Ref. 4.

[7] S. L. Thomson and H. S. Lauson (1972) as discussed in Ref. 4.

[8] M. H. Rice, J. Phys. Chem. Solids **26**, 483 (1965).

[9] E. Royce (1971) as discussed in Ref. 4.

[10] O. L. Anderson, J. Geophys. Res. **84**, 3537 (1979).

[11] S. K. Srivastava and P. Sinha, Physica B **404**, 4316-4320 (2009).

[12] R. Jeanloz, J. Geophys. Res. **94(B5)**, 5873-5886 (1989).

[13] L. V. Al'tshuler and I. I. Sharipdzhanov, Izvestiya Akad. Nauk SSSR, Fizika Zemli **3**, 11 (1971) [Izv. Acad. Sci. USSR, Earth Physics **3**, 167 (1971)].

[14] A. V. Bushman, I. V. Lomonosov, V. E. Fortov, and K. V. Khishchenko, Zh. Eksp. Teor. Fiz. **109**, 1662-1670 (1996) [JETP **82**, 895 (1996)]; K. V. Khishchenko, Journal of Physics: Conference Series **653** 012081 (2015); doi:10.1088/1742-6596/653/1/012081

[15] F. D. Stacey and P. M. Davis, Phys. Earth Planet. Int. 142, 137 (2004).

[16] P. I. Dorogokupets and A. Dewaele, High Pressure Research **27**, 431 (2007).

[17] B. L. N. Kennett and I. Jackson, Phys. Earth Planet. Inter. **176**, 98 (2009);

[18] K. D. Litasov et al., J. Appl. Phys. **113**, 093507 (2013), Table IV.

[19] Y. Aizawa and A. Yoneda, Phys. Earth Planet. Inter. **155**, 87 (2006).

[20] T. S. Sokolova, P. I. Dorogokupets, and K. D. Litasov, Russian Geology and Geophysics **54**, 181 (2013).

[21] V. N. Zharkov, Phys. Earth Planet. Inter. **109**, 79-89 (1998).

[22] Y. Tange, Y. Nishihara, and T. Tsuchiya, J. Geophys. Res. **114**, B03208 (2009).

[23] S. S. Kushwah and M. P. Sharma, Solid State Commun. 152, 414 (2012).

[24] Zhang and Sun, Chin. Phys. B Vol. 21, No. 8 (2012) 080508

[25] S. Spetziale, C. S. Zha, T. S. Duffy, R. J. Hemley, and H. K. Mao, J. Geophys. Res. **106**, 515 (2001).

[26] S. P. Marsh, *LASL Shock Hugoniot Data* (University of California Press, Berkeley, 1980).

[27] D. E. Fratanduono, J. H. Eggert, M. C. Akin, R. Chau, and N. C. Holmes, J. Appl. Phys. **114**, 043518 (2013).

[28] M. S. Vassiliou and T. J. Ahrens, Geophys. Res. Lett. 8, 729 (1981).

[29] L. Zhang, Z. Gong, and Y. Fei, J. Phys. Chem. Solids **69**, 2344 (2008).

[30] M. W. Chase, Jr., NIST-JANAF Thermochemical Tables, 4th edition. Journal of Physical and Chemical Reference Data, Monograph **9** (1998), p. 1536.

[31] K. Wang and R. R. Reeber, in *Computer-Aided Design of High-Temperature Materials*, edited by A. Pechenik, R. K. Kalia, and P. Vashishta (Oxford University Press, New York, New York, 1999), p. 473.

[32] S. K. Saxena and G. Sheng, J. Geophys. Res. **97**, 19813 (1992).

[33] M. H. G. Jacobs and H. A. J. Oonk, Calphad **24**, 133 (2000); Phys. Chem. Chem. Phys. **2**, 2641 (2000); S. Raju, E. Mohandasa, and K. Sivasubramanian *ibid.* **3**, 1391 (2001).

[34] L. S. Dubrovinsky and S. K. Saxena, Phys Chem Minerals **24**, 547 (1997).

[35] G. Fiquet, P. Richet, and G. Montagnac, Phys. Chem. Minerals **27**, 103 (1999).

[36] M. H. G. Jacobs and H. W. S. de Jong, Phys. Chem. Chem. Phys. **5**, 2056 (2003).

[37] W. J. Carter, S. P. Marsh, J. N. Fritz, and R. G. McQueen, "The equation of state of selected materials for high-pressure references," in *Accurate Characterization of the High-Pressure Environments*, Spec. Publ., 326E. C. Lloyd, pp. 147-158, National Bureau of Standards, Washington, D.C., (1971).

[38] A. M. Molodets, Fizika Goreniya i Vzryva **42**, 110 (2006) [Combustion, Explosion and Shock Waves **42**, 346 (2006)].

[39] Caloric EOS description: I. V. Lomonosov, A. V. Bushman, V. E. Fortov, and K. V. Khishenko, *Caloric equations of state of structural materials*, AIP Conf. Proc. **309**, 133 (1994); Shock-wave database info: P. R. Levashov, K. V. Khishenko, I. V. Lomonosov, and V. E. Fortov, *Database of Shock-Wave Experiments and Equations of State Available via Internet*, AIP Conf. Proc. **706**, 87 (2004); Primary input experimental data are available at: *http://www.ihed.ras.ru/rusbank/substsearch.php* (seach for "periclase", then select and click on

"get data").

[40] Y. Sumino, O. L. Anderson, and I. Suzuki, Phys. Chem. Minerals **9**, 38 (1983).

[41] D. G. Isaak, O. L. Anderson, and T. Goto, Phys. Chem. Minerals **16**, 704 (1989).

[42] E. S. Zouboulis and M. Grimsditch, J. Geophys. Res. **96**, 4167 (1991).

[43] S. Root, L. Shulenburger, R. W. Lemke, D. H. Dolan, T. R. Mattsson, and M. P. Desjarlais, Phys. Rev. Lett. **115**, 198501 (2015), supplementary material.